



Drying tendency over the southern slope of the Tibetan Plateau in recent decades: role of a CGT-like atmospheric change

Ziqian Wang^{1,2} · Song Yang^{1,2} · Haolin Luo¹ · Jiandong Li³

Received: 8 November 2021 / Accepted: 12 March 2022 / Published online: 27 March 2022
© The Author(s) 2022

Abstract

A significant drying tendency over the southern slope of the Tibetan Plateau (SSTP) in summer (especially in July–September) during 1980–2018 is identified in this study. Moisture budget analysis reveals that the drying tendency is dominated by a decreased vertical moisture advection due to weakened upward motion, which is mainly resulted from an anticyclonic trend appeared over the northeastern TP. This anomalous anticyclone can weaken the upper-tropospheric divergence pumping over the SSTP. In addition, moist static energy diagnosis indicates that the southern branch of the anomalous anticyclone advects low moist enthalpy air into the SSTP, which also suppresses local upward motion and convection. Moreover, the anticyclonic trend over the northeastern TP is found not a local phenomenon, but is rather associated with the large-scale atmospheric change in the middle latitudes that shows a circumglobal teleconnection (CGT)-like pattern. Our results highlight that the long-term CGT-like trend of atmospheric circulation plays a crucial role in triggering the drying tendency over the SSTP in recent decades.

Keywords Drying trend · Tibetan Plateau · CGT-like pattern · Moisture · Moist static energy analyses

1 Introduction

The Tibetan Plateau (TP), located in the subtropical central-eastern Eurasian continent, is the highest and largest plateau in the world. Due to the lifting effect of the steep southern slope of the TP (SSTP) through both thermal and mechanical forcings, the northern branch of the South Asian summer monsoon forms over the southern TP (Wu et al. 2012). Corresponding with the strongest upward motion, a large rainfall center always appears over the SSTP during the monsoon season (Wang et al. 2016). Known as the “Asian

Water Tower” (Lu et al. 2005; Xu et al. 2008), the TP is the source region of many large rivers such as the Ganges, the Indus, the Mekong, the Brahmaputra, the Yangtze River, and the Yellow River. These water resources have been sustaining the industrial, agricultural, and living usages of water for nearly 40% of the world’s population (Xu et al. 2008). Precipitation is one of the most important components in the hydrological cycle over the TP, and its variations directly regulate the streamflow of the major Asian rivers (Zhang et al. 2013). Moreover, precipitation releases huge condensational heat and changes local atmospheric heat source over the TP, especially along the southern Himalayas in the monsoon season, which drives nearby large-scale circulation and further remotely influences the weather and climate in many places of the world (e.g., Zhao and Chen 2001; Hsu and Liu 2003; Kitoh 2004; Duan et al. 2012; Wu et al. 2016c; Lu et al. 2018, 2019). Understanding the physical processes responsible for the precipitation change over the TP is of great societal and scientific importance.

Much effort has been devoted to identifying the inter-annual variability of TP precipitation, which is influenced by both tropical forcing and mid-latitude atmospheric teleconnection (e.g., Liu and Yin 2001; Liu et al. 2015, 2021; Wang et al. 2017b; Jiang and Ting 2017; Hu et al. 2021).

✉ Ziqian Wang
wangziq5@mail.sysu.edu.cn

¹ School of Atmospheric Sciences, Sun Yat-sen University, and Southern Marine Science and Engineering Guangdong Laboratory (Zhuhai), Zhuhai, China

² Guangdong Province Key Laboratory for Climate Change and Natural Disaster Studies, Sun Yat-sen University, Zhuhai, China

³ State Key Laboratory of Numerical Modeling for Atmospheric Sciences and Geophysical Fluid Dynamics, Institute of Atmospheric Physics, Chinese Academy of Sciences, Beijing, China

With the growing interest in global climate change/warming, the long-term trend of precipitation over the TP has become a hot research topic. Different from the uniformly warming trend over the whole TP, the change in precipitation shows obvious spatial discrepancies (Yao et al. 2012; Gao et al. 2014). It is found that the TP is getting wetter as a whole, particularly in the western-central TP, i.e. the Inner TP (Li et al. 2010; You et al. 2015; Zhang et al. 2017a; Sun et al. 2020). The rapid lake expansion in the recent decades attests the robust precipitation increase in the Inner TP, showing not only the increased area of original lakes (such as Selin Co and Nam Co) and also the increased number of new lakes ($> 1 \text{ km}^2$) (Zhang et al. 2017b, 2019). However, previous studies indicated that precipitation exhibited decreasing trend along the TP periphery (Duan et al. 2011; Yang et al. 2014; Gao et al. 2015), although the statistical significance of the trend could be high or low if the different time period considered. Duan et al. (2011) attributed the precipitation decreasing along the southern and eastern slopes to the weakened surface sensible heating over the TP. However, to a larger extent, it is difficult to clarify the causal relationship between local sensible heating and precipitation (latent heating) due to their intense interactions (Wu et al. 2016b). On the other hand, Yang et al. (2014) concluded that the weakened Asian monsoon was responsible for the less precipitation in the marginal area of the TP during 1984–2006. Indeed, the rainfall trend in the Asian monsoon region presents significant spatial discrepancies (Duan et al. 2011). Wang and Gillies (2013) reported that the Himalayan “mountain rain belt” was inhomogeneous to the all-India monsoon rainfall. Meanwhile, an analysis of several monsoon indices shows no significantly weakened trends in the recent decades (figure not given). Recently, Yue et al. (2020) reported that the summer precipitation in the southern TP featured a decadal variation with a peak of around 10 years and a downward trend appearing after 1998. They attributed this feature to the impact from the dipolar pattern of sea surface temperature between the equatorial central Pacific and the Indo-Pacific warm pool.

We revisit the long-term changes in summer precipitation along the TP periphery using multi-source datasets. Consistently in all observational data, a significant drying trend is seen over the SSTP region (Fig. 1), where the climatological rainfall center is located (Fig. S1a in Supplementary Information). It should be pointed out that the highly-populated Ganges Valley, the largest river in the South Asian subcontinent, is also located in this region. Thus, a better understanding of the change in SSTP precipitation is very important in many ways. Our findings in this study raise an intriguing possibility that the long-term change of atmospheric circulation in middle latitudes distinctly contributes to the drying tendency over the SSTP. We will uncover this possible

contribution and the detailed physical mechanisms involved from dynamic diagnoses.

The remainder of this paper is organized as follows. In Sect. 2, the data and methodology are described briefly. Section 3 presents the results of data analysis and dynamic diagnosis, and clarifies the physical mechanisms for the drying tendency over the SSTP. Finally, a further discussion and brief conclusion are provided in Sect. 4.

2 Data and methodology

The monthly precipitation observations employed in this study include two widely-used gridded datasets: the Global Precipitation Climatology Project version 2.3 (GPCP; Adler et al. 2003) with a $2.5^\circ \times 2.5^\circ$ horizontal resolution, and the Global Precipitation Climatology Centre (GPCC; Schneider et al. 2014) full data reanalysis version 7 at a horizontal resolution of $1.0^\circ \times 1.0^\circ$. The GPCC is based on the quality-controlled raingauge data and available only over land, while the GPCP is a combination of satellite and station observations and covers global land and oceans. The long-term Japanese 55-year Reanalysis (JRA-55; Kobayashi et al. 2015) dataset is used for atmospheric diagnosis. This dataset extends from 1000 to 1 hPa, with a horizontal resolution of $1.25^\circ \times 1.25^\circ$. The JRA-55 is chosen because it can well replicate the drying trend over the SSTP (see Fig. 1). Our analysis is focused on the mid-late summer (July, August, and September, JAS hereafter) during the period of 1980–2018. In addition, two more observed precipitation datasets derived from the Asian Precipitation Highly Resolved Observational Data Integration toward Evaluation of Water Resources (APHRODITE; Yatagai et al. 2012) in 1980–2015 and the Tropical Rainfall Measuring Mission (TRMM; Huffman et al. 2007) in 1998–2018 are also adopted here for the supporting investigation in the supplementary materials.

To better understand the observational result, model output from the Community Earth System Model Large Ensemble (CESM-LE) project is applied (Kay et al. 2015). This project includes a 40-member ensemble of fully-coupled CESM1 simulations for 1920–2100 at a horizontal resolution of $1^\circ \times 1^\circ$. Each member is subject to the same radiative forcing scenario (historical before 2005 and RCP8.5 thereafter) and is only slightly perturbed in the initial atmospheric state. As popularly applied previously (e.g., Ding et al. 2017; Hui and Zheng 2018), the CESM-LE project is designed as facilitating the analysis of climate change and internal variability.

A moisture budget analysis, suitable for the TP and surrounding area (e.g., Wang et al. 2017b; Peng and Zhou 2017; He et al. 2019), is adopted here to understand the mechanisms for the drying trend over the SSTP.

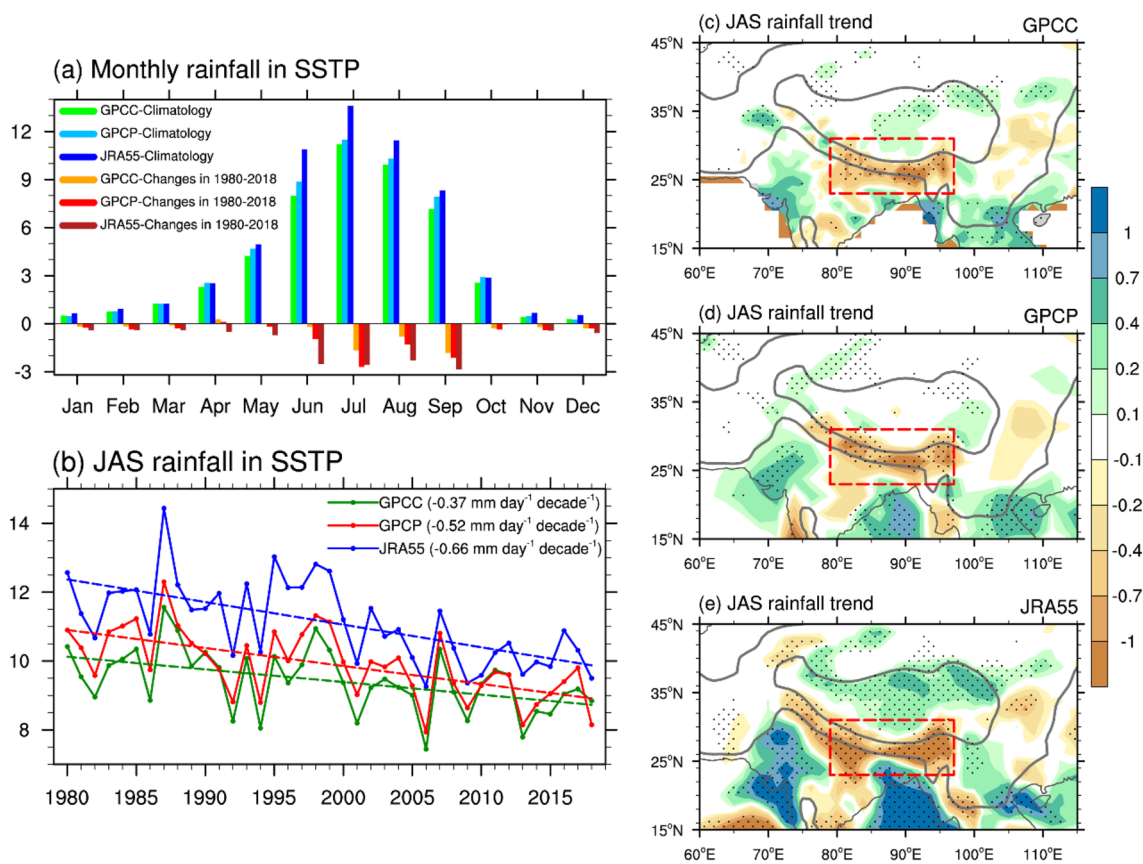


Fig. 1 **a** Climatology (bars with cold colors; mm day^{-1}) and changes (bars with warm colors; mm day^{-1}) of the monthly rainfall averaged over the SSTOP area (red boxes in **c–e**; $79^{\circ}\text{--}97^{\circ}\text{E}$, $23^{\circ}\text{--}31^{\circ}\text{N}$) for 1980–2018 based on GPCP, GPCP, and JRA-55, respectively. **b** Time series of the mean rainfall (mm day^{-1}) in JAS over the SSTOP area. Dashed lines are the corresponding long-time linear trends, and the

magnitudes of linear trends are marked. **c** Linear trend ($\text{mm day}^{-1} \text{decade}^{-1}$) of GPCP rainfall in JAS, in which the stippling indicates the significant values $>95\%$ confidence level and the bold gray contours denote the topographic heights of 500 m and 3000 m. **d** Same as **c**, but for the GPCP data. **e** Same as **c**, but for the JRA-55

Following He et al. (2019), the formula of moisture budget is expressed as

$$P' = E' - \langle \overline{\omega} \partial_p q' \rangle - \langle \omega' \partial_p \bar{q} \rangle - \langle \bar{\mathbf{V}} \cdot \nabla_h q' \rangle - \langle \mathbf{V}' \cdot \nabla_h \bar{q} \rangle + R, \tag{1}$$

where P , E , ω , \mathbf{V} , q , and R denote precipitation, evaporation, vertical p -velocity, horizontal wind, specific humidity, and the residual, respectively. ∇_h is the horizontal differential operator, and the subscript p represents vertical direction at p level coordination. The variables with a prime indicate the monthly anomaly, and those with an overbar denote the climatological mean during the period of 1980–2018. The symbol $\langle \rangle$ indicates the vertical integration from the surface to 100 hPa. Therefore, the change in precipitation is determined by evaporation change, thermodynamic and dynamic changes in vertical moisture advection, thermodynamic and dynamic changes in horizontal moisture advection, and the residual term on the right of Eq. (1).

As will be shown in Sect. 3.1, the dry tendency over the SSTOP is primarily caused by the weakened upward motion. To investigate the mechanisms responsible for the anomalous vertical motion, we further diagnose the moist static energy (MSE) budget (Neelin and Held 1987; Wu et al. 2017), which was considered as one of the dominant theoretical paradigms for understanding monsoon rainfall (Hill 2019). The equation can be written as

$$\partial_t \langle C_p T + L_v q \rangle' + \langle \mathbf{V} \cdot \nabla_h (C_p T + L_v q) \rangle' + \langle \omega \partial_p h \rangle' = F'_{net}, \tag{2}$$

where F_{net} is the net flux into the atmospheric column from the surface and the top of atmosphere. MSE is denoted by $h = C_p T + L_v q + \phi$; T is air temperature; ϕ is the geopotential; C_p and L_v are the specific heat at constant pressure and the latent heat of vaporization, respectively; and $C_p T + L_v q$ is the moist enthalpy. The other symbols in Eq. (2) are identical with Eq. (1). Due to the seasonal mean time tendency term

$(\partial_t \langle C_p T + L_v q \rangle')$ is relatively small and can be neglected, the MSE equation can be simplified to

$$\langle \omega' \partial_p \bar{h} \rangle = F'_{net} - \langle \bar{\omega} \partial_p h' \rangle - \langle \mathbf{V}' \cdot \nabla_h \overline{(C_p T + L_v q)} \rangle - \langle \bar{\mathbf{V}} \cdot \nabla_h (C_p T + L_v q)' \rangle + R. \quad (3)$$

According to the previous studies (e.g., Back and Bretherton 2006; Wu et al. 2017; Hu et al. 2021), in the tropics and subtropical monsoon regions (such as the SSTP) with deep convection in summer, the gross moist stability is generally positive and the $\partial_p \bar{h}$ is usually less than 0, then the negative terms on the right-hand side of Eq. (3) can arouse anomalous descending motion ($\omega' > 0$) under the constraints of the MSE budget balance.

Additionally, the methodology also includes the linear correlation analysis and regression analysis. The Student's t test is applied to assess the statistical significance of the results obtained.

3 Results

3.1 Drying tendency over the SSTP and moisture budget analysis

As discussed in the introduction, the northern branch of the South Asian summer monsoon develops over the SSTP area, characterized by heavy rainfall and strong upward motion (see the supplementary Fig. S1). The SSTP area (79° E–97° E, 23° N–31° N) being focused in our analysis exactly covers the monsoon rainfall center in climatology, and it shows the most significant drying tendency (Fig. 1c–e) to be discussed.

Figure 1a shows the climatology and the changes in monthly precipitation amount averaged in the SSTP for 1980–2018 based on three datasets. A major portion of precipitation (~75% of the annual total amount) occurs from June to September, corresponding with the time of South Asian summer monsoon. Almost all of these months experience a drying tendency during the analysis period, although different trends could appear in various months due to data discrepancy and other factors. Except June when a slight drying change appears in GPCC, July, August, and September commonly present an obvious decrease of precipitation in the three datasets. Hereinafter, we focus on the JAS mean and analyze the feature of drying tendency over the SSTP. Nevertheless, including June will not change the main conclusions of our study. According to the spatial distributions of the linear trends of JAS mean precipitation (Fig. 1c–e), three datasets consistently show significantly decreased precipitation over the slope area, where the topography rises sharply from below 500 m to 3000 m. The temporal variations of SSTP-averaged JAS precipitation are shown in Fig. 1b. All the time series reveal significant downward

trends, $-0.37 \text{ mm day}^{-1} \text{ decade}^{-1}$, $-0.52 \text{ mm day}^{-1} \text{ decade}^{-1}$, and $-0.66 \text{ mm day}^{-1} \text{ decade}^{-1}$ for GPCC, GPCP, and JRA-55, respectively, which are all statistically significant at the 99% confidence level. An estimate from the mean of three datasets indicates that the JAS rainfall over the SSTP has decreased by ~20% during 1980–2018. Furthermore, two more datasets derived from the APHRODITE project (Yatagai et al. 2012) in 1980–2015 and the TRMM (Huffman et al. 2007) in 1998–2018 confirm the significant drying tendency over the SSTP, although the time periods are different (Fig. S2 in Supplementary Information). This drying trend directly results in decreases in lake area and runoff that have been observed in the TP's southern periphery (Yang et al. 2014; Zhang et al. 2019), and more likely exerts a negative influence on the water resource for human activities in the surrounding countries. For example, vanishing springs in the Nepalese mountains have been reported, accompanied by drying drinking water sources, low crop yields, and forest degradation in Nepal (Poudel and Duex 2017).

To understand the dominant contributor to the SSTP drying tendency, atmospheric moisture budget is diagnosed according to Eq. (1). The JRA-55 reanalysis dataset is adopted because of its reasonable replication of the observed drying trend, although the magnitude is somewhat stronger (Fig. 1b, e). Figure 2 shows the changes per decade of the first five terms on the right-hand side of Eq. (1). It is clearly seen that the dynamic change in vertical moisture advection ($-\langle \omega' \partial_p \bar{q} \rangle$) is the largest contributor to the decreased precipitation over the SSTP (Fig. 2c). By comparison, the other four terms all exhibit small values in the slope region. In Fig. 2c, the spatial pattern of the obviously weakened dynamic component in vertical moisture advection is remarkably consistent with the pattern of decreased precipitation (Fig. 1e). Moreover, the various components of the area-averaged moisture budget are shown in Fig. 2f, further confirming the overriding contribution from the term $-\langle \omega' \partial_p \bar{q} \rangle$ with the negative value even larger than that of precipitation change. The above moisture budget analysis, demonstrating the dynamic change in vertical moisture advection as the responsible factor for the drying tendency over the SSTP, indicates the dominance of the change in vertical motion (ω' in Eq. (1)).

Furthermore, a simple recycling equation developed from the above traditional atmospheric moisture budget (details refer to Zangvil et al. (2004)) is also diagnosed here. The relative contributions of locally evapotranspired moisture versus externally advected water vapor for the SSTP drying tendency are estimated (figure not shown). This diagnose confirms no impact from the change of local evaporation, while the main contribution for the drying SSTP comes from the remarkable reduction of the external moisture inflow at the southern boundary of the SSTP

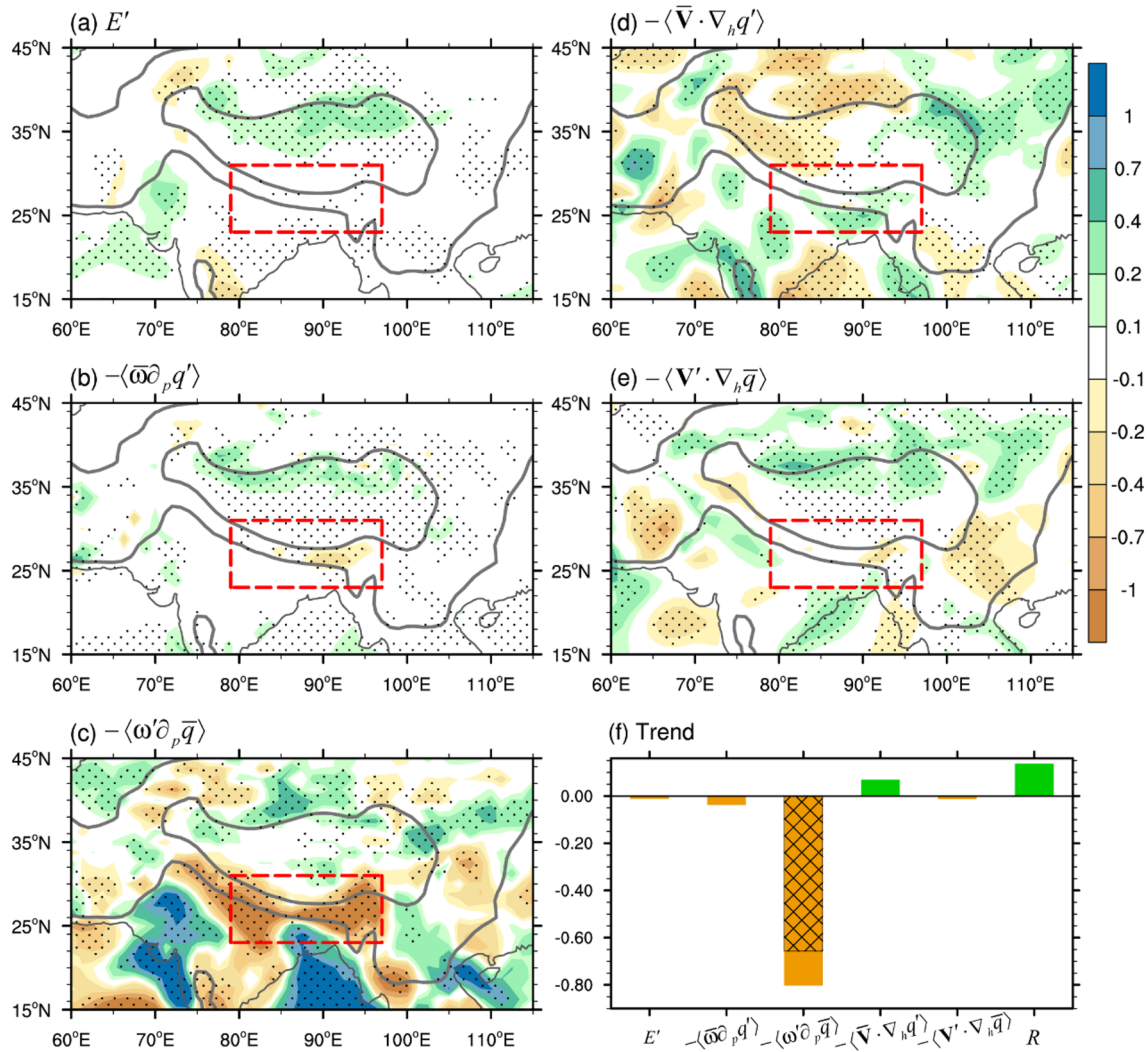


Fig. 2 Changes ($\text{mm day}^{-1} \text{ decade}^{-1}$) in the first five terms on the right-hand side of Eq. (1) based on JRA-55 in JAS for 1980–2018: **a** evaporation, **b** thermodynamic component of vertical moisture advection, **c** dynamic component of vertical moisture advection, **d** thermodynamic component of horizontal moisture advection, and **e** dynamic component of horizontal moisture advection. In **f**, color bars are the

corresponding area-averaged values of each term over the SSTP area ($79^\circ \text{ E}–97^\circ \text{ E}$, $23^\circ \text{ N}–31^\circ \text{ N}$), and the cross-slash bar is the change in precipitation. In **a–e**, the stippling indicates the significant values $>95\%$ confidence level and the bold gray contours denote the topographic heights of 500 m and 3000 m

region. Climatologically, the southern boundary is the only channel for water vapor mass inflow into the SSTP region, pumped by the strong upward motion over the slope region (Fig. S1b). This pumping effect is significantly weakened in past decades over the SSTP (to be discussed in the next section), which reduces the moisture inflow into the SSTP region transporting from the southern tropical ocean, further highlighting the important role of dynamic change in vertical moisture advection ($-\langle \omega' \partial_p \bar{q} \rangle$ in Eq. (1)).

3.2 Physical mechanism for the change of vertical motion over the SSTP

The question needs to be addressed now is why the vertical motion over the SSTP changes during 1980–2018. Climatologically, there exists a powerful anticyclone over the southern TP in summer, known as the South Asian High (Mason and Anderson 1963), which can provide the upper-level air pumping effect via a significant divergence center (Fig. 3a; Liu et al. 2013). This pumping effect is crucial for the formation and maintenance of strong upward motion over the SSTP (Fig. 3c). Meanwhile, the Asian subtropical westerly jet in summer is coincident with the northern edge

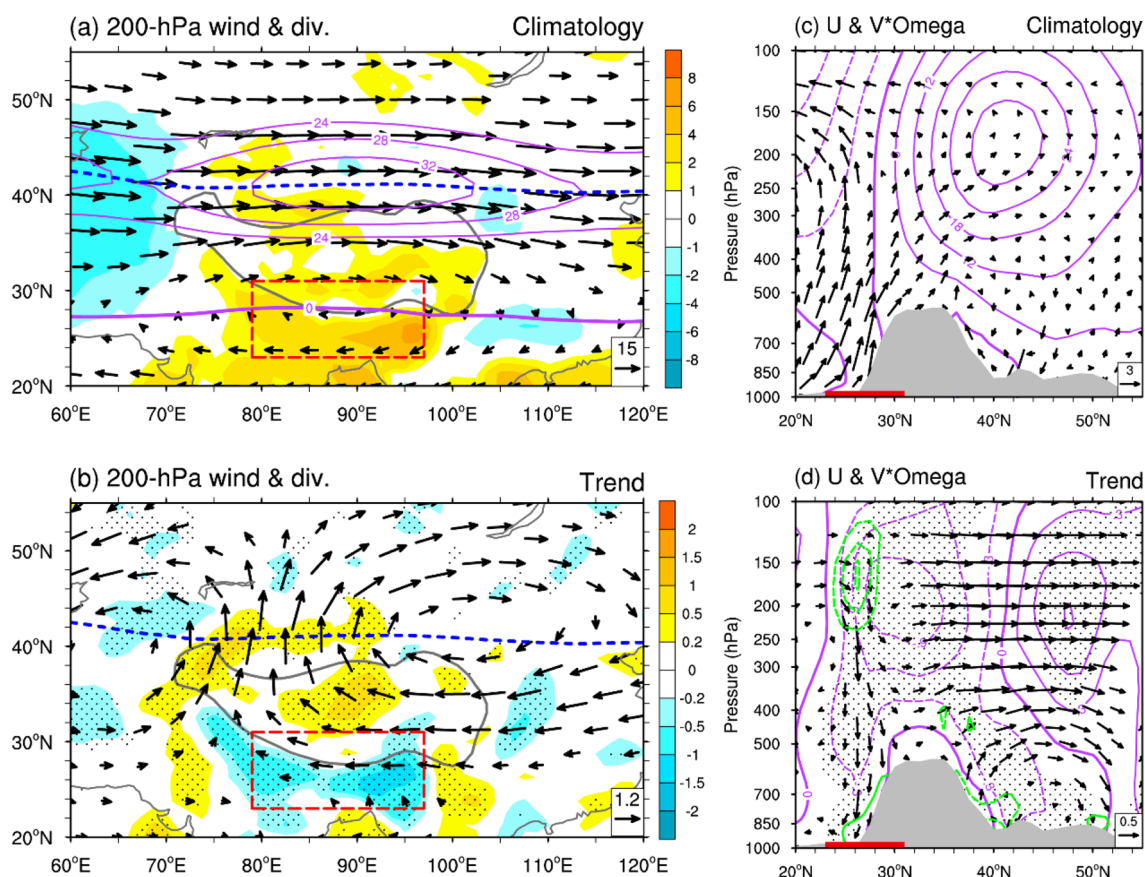


Fig. 3 **a** Climatology of 200-hPa zonal wind (solid contours; m s^{-1}), horizontal wind (vectors; m s^{-1}), and divergence (shading; 10^{-6} s^{-1}) in JAS for 1980–2018. **b** Same as **a**, but for the linear trends of horizontal wind ($\text{m s}^{-1} \text{ decade}^{-1}$) and divergence ($10^{-6} \text{ s}^{-1} \text{ decade}^{-1}$), in which the stippling indicates the significant values >95% confidence level for divergence trend, and only the significant vectors >95% confidence level are plotted. In **a**, **b**, the dashed blue curve is the JAS climatological westerly jet axis, and the bold gray contours denote the topographic height of 3000 m. **c** Pressure-latitude cross section of climatological zonal wind (contours; m s^{-1}) and vertical circula-

tion (vectors; v in m s^{-1} , ω in 0.02 Pa s^{-1}) averaged from 79° E to 97° E , in which gray shading denotes the terrain. **d** Same as **c**, but for the linear trends of zonal wind and vertical circulation per decade, in which green contours show the linear trend of divergence field with absolute value ≥ 0.4 (dashed is negative, and solid is positive; $\text{CI} = 0.4 \times 10^{-6} \text{ s}^{-1} \text{ decade}^{-1}$), the stippling indicates the significant values >95% confidence level for zonal wind trend, and only the significant vectors >95% confidence level for vertical circulation trend are plotted

of the South Asian High (Fig. 3a). Specifically, the junction of tropical easterly flow and subtropical westerlies is located over the SSTP, corresponding with the aforementioned significant upper-level divergence and upward motion (Fig. 3a, c). Thus, any variations in upper-level atmospheric circulation can directly regulate the divergence pumping, which will further influence the intensity of upward motion over the SSTP area.

During 1980–2018, the long-term trend of upper-level atmospheric circulation presents an anomalous anticyclone over the northeastern TP centered along the climatological westerly jet ($\sim 40^\circ \text{ N}$) and is located at the northeastern flank of the South Asian High (Fig. 3b). The pressure-latitude cross section of the linear trend of zonal wind (Fig. 3d) clearly shows a significant equivalent barotropic feature in the anomaly anticyclone, with a maximum

intensity at about 200 hPa. Uniform easterly anomalies appear over the TP (Fig. 3b, d), which are inverse with the climatological westerlies (Fig. 3a) and evidently reduce the upper-level divergence (Fig. 3b). This weakened divergence is manifested by the deep convergence tendency between 250 and 100 hPa over the SSTP (shown by the green dashed contours in Fig. 3d), suggesting an attenuated upper-level pumping effect. Consequently, the upward motion is weakened (Fig. 3d), leading to the weakened vertical moisture advection (Fig. 2c) and decreased precipitation over the SSTP. It is worth mentioning that the trend of divergence in the lower level is much weaker compared with the upper-level significant and deep convergence tendency (Fig. 3d). This phenomenon further highlights the dominant effect due to the change in the upper-level atmospheric circulation.

Simulations from the CESM-LE project are adopted to confirm the relationship between the upper-level anomaly anticyclone and the SSTP drying tendency. The 40-member ensemble mean displays almost no trend in JAS precipitation over the SSTP during 1980–2018 (Fig. 4a). Since the multi-member ensemble mean can effectively suppress the internal variability and isolate the effect of external forcing (Kay et al. 2015), we speculate that the observed SSTP drying tendency is probably regulated by atmospheric internal variability, instead of anthropogenic forcing. Among the 40 members of the CESM-LE project, four members are detected to simulate a significant drying trend over the SSTP successfully (Fig. 4b). These cases show the common changes in the upper-level atmospheric circulations (Fig. 4c, d), namely significant anomalous anticyclone with a barotropic structure over the northeastern TP. Moreover, there exists an upper-level significant and deep (250–100 hPa) convergence trend over the SSTP in the drying CESM-LE cases (Fig. 4d), while a weak signal in the lower level. This point is identical with the observed result shown in Fig. 3d, again confirming the more important role of the change in the upper-level

atmospheric circulation, which is favorable for the weakened upward motion.

In the tropics or monsoon regions, the vertical motions are constrained by the MSE budget balance (e.g., Neelin et al. 2003; Chou and Neelin 2004; Wu et al. 2017; Hu et al. 2021). We diagnose the MSE equation (Eq. (3)) to further verify the physical processes causing the anomalous descending motion over the SSTP (Fig. 3d) under the influence of upper-level anticyclonic change. According to the methodological introduction in Sect. 2, the negative terms on the right-hand side of Eq. (3) can arouse anomalous descending motion. Result indicates that the advection of climatological moist enthalpy by anomalous horizontal wind ($-\langle \mathbf{V}' \cdot \nabla_h (C_p T + L_v q) \rangle$) has the largest contribution to the weakened upward motion over the SSTP in recent decades (Fig. 5). To explore the detailed process of this term, a further decomposition is applied (Fig. 6). For the climatology, both the atmospheric specific humidity and temperature peak in the middle-upper troposphere over the SSTP (Fig. 6a), supporting the plateau as a moist and warm center in summer (e.g., Ye and Wu 1998; Xu et al. 2008; Boos and Kuang 2010). With the

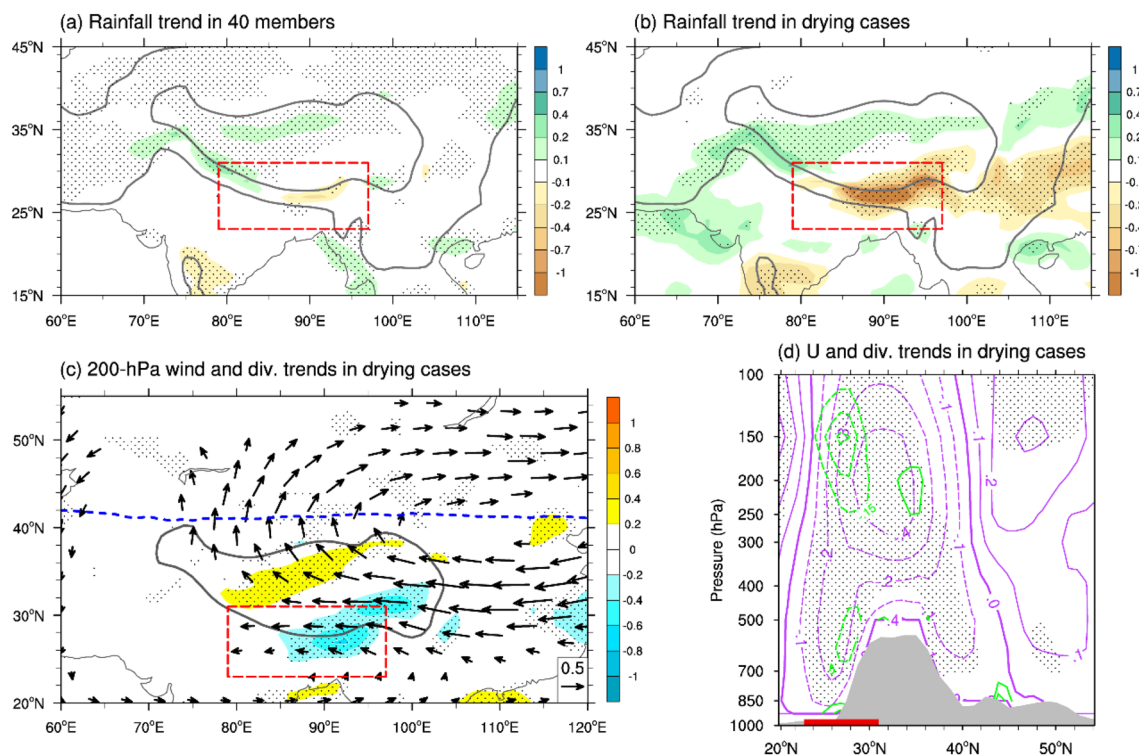


Fig. 4 **a** Linear trend ($\text{mm day}^{-1} \text{decade}^{-1}$) of the 40-member ensemble mean rainfall from the CESM-LE project in JAS of 1980–2018. **b** Same as **a**, but for the mean of drying cases in the CESM-LE 40 members. **c** Same as **b**, but for the 200-hPa divergence (shading, 10^{-6} s^{-1}) and wind (vectors; $\text{m s}^{-1} \text{decade}^{-1}$), in which the dashed blue curve is the JAS climatological westerly jet axis. **d** Same as **c**, but for the pressure-latitude cross sections of zonal wind (orchid

contours; $\text{m s}^{-1} \text{decade}^{-1}$) and divergence field with absolute value ≥ 0.15 (green contours; dashed is negative and solid is positive; $\text{CI} = 0.15 \times 10^{-6} \text{ s}^{-1} \text{decade}^{-1}$) averaged from 79°E to 97°E . The stippling indicates the significant values $> 95\%$ confidence level for rainfall in **a**, **b**, divergence in **c**, and zonal wind in **d**. The bold gray contours denote the topographic heights of 500 m and 3000 m in **a**, **b** and 3000 m in **c**, and gray shading denotes the terrain in **d**

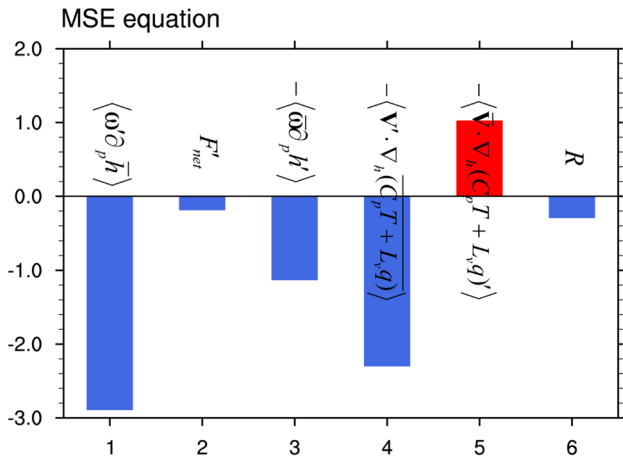


Fig. 5 Linear trends ($\text{W m}^{-2} \text{decade}^{-1}$) for each term of the MSE equation (Eq. (3)) based on the JRA-55 in JAS during 1980–2018, being calculated by the area-averaged values over the SSTP area (79°E – 97°E , 23°N – 31°N)

influence of anomalous anticyclonic trend over the northeastern TP in 1980–2018, the anomalous easterlies at the anticyclone’s southern flank obviously bring the cold and dry (low moist enthalpy) air advecting into the region of SSTP (Fig. 6a). Driving by the anomalous horizontal wind, the anomalous cold air advection ($-\langle \mathbf{V}' \cdot \nabla_h(C_p \bar{T}) \rangle$; Fig. 6b), in comparison with the anomalous dry air advection ($-\langle \mathbf{V}' \cdot \nabla_h(L_v \bar{q}) \rangle$; Fig. 6c), presents the dominated contribution to the negative horizontal advection of climatological moist enthalpy ($-\langle \mathbf{V}' \cdot \nabla_h(C_p \bar{T} + L_v \bar{q}) \rangle$) over the SSTP (Fig. 5). Therefore, the above MSE budget diagnosis again demonstrates that the anomalous anticyclonic trend over the northeastern TP is the key system weakening the upward motion over the SSTP through advecting the low moist enthalpy air into the slope area.

It should be noted that, except for the most important contribution from $-\langle \mathbf{V}' \cdot \nabla_h(C_p \bar{T} + L_v \bar{q}) \rangle$ on the weakened upward motion over the SSTP, the term $-\langle \overline{\omega \partial_p h'} \rangle$ is also negative with a relatively small value (Fig. 5). Namely, the vertical advection of anomalous MSE by climatological vertical motion also contributes to the weakened upward motion over the SSTP in recent decades. This term is mainly related to the change in the vertical structure of the MSE h' (Wu et al. 2017), which is primarily regulated by the subcomponent of latent energy $L_v q'$ (see the supplementary Fig. S3). The positive trend of moisture content or latent energy over the SSTP presents a vertical structure with a maximum at about 550 hPa (Fig. S3b), which is probably connected to the enhanced warming at middle troposphere resulted from the increasing elevated aerosol loading over the Indo-Gangetic Plain and Himalayan foothills in recent decades (Li et al. 2016). Since the key role of anomalous anticyclone over the northeastern TP is focused here, the detailed process for the

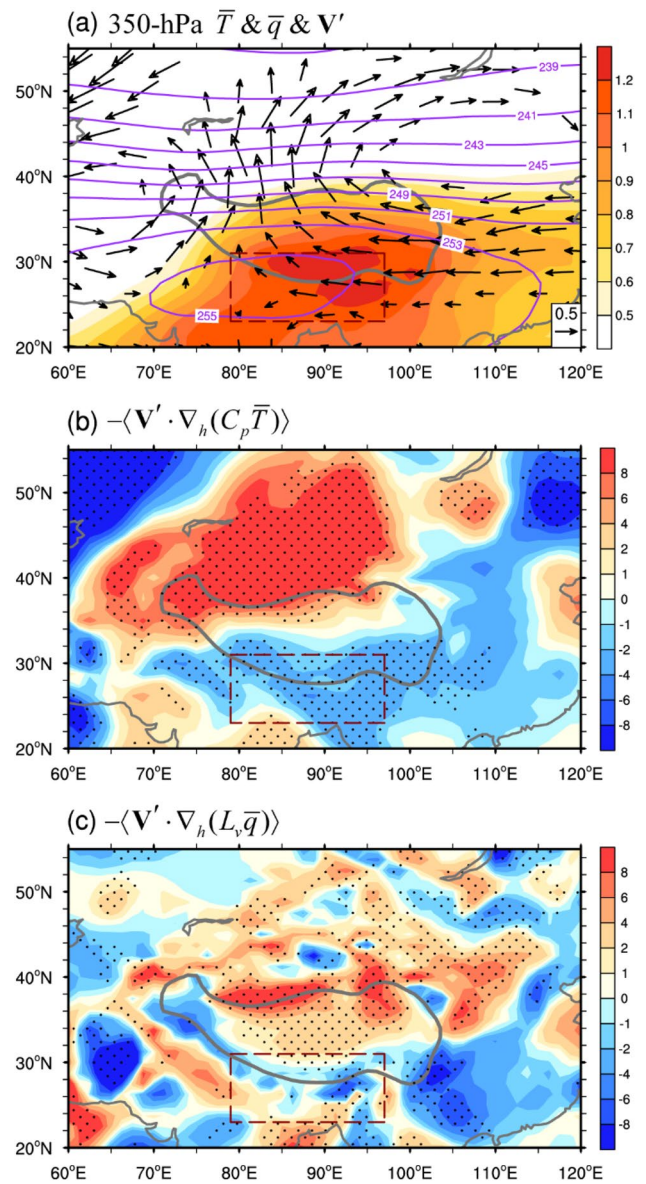


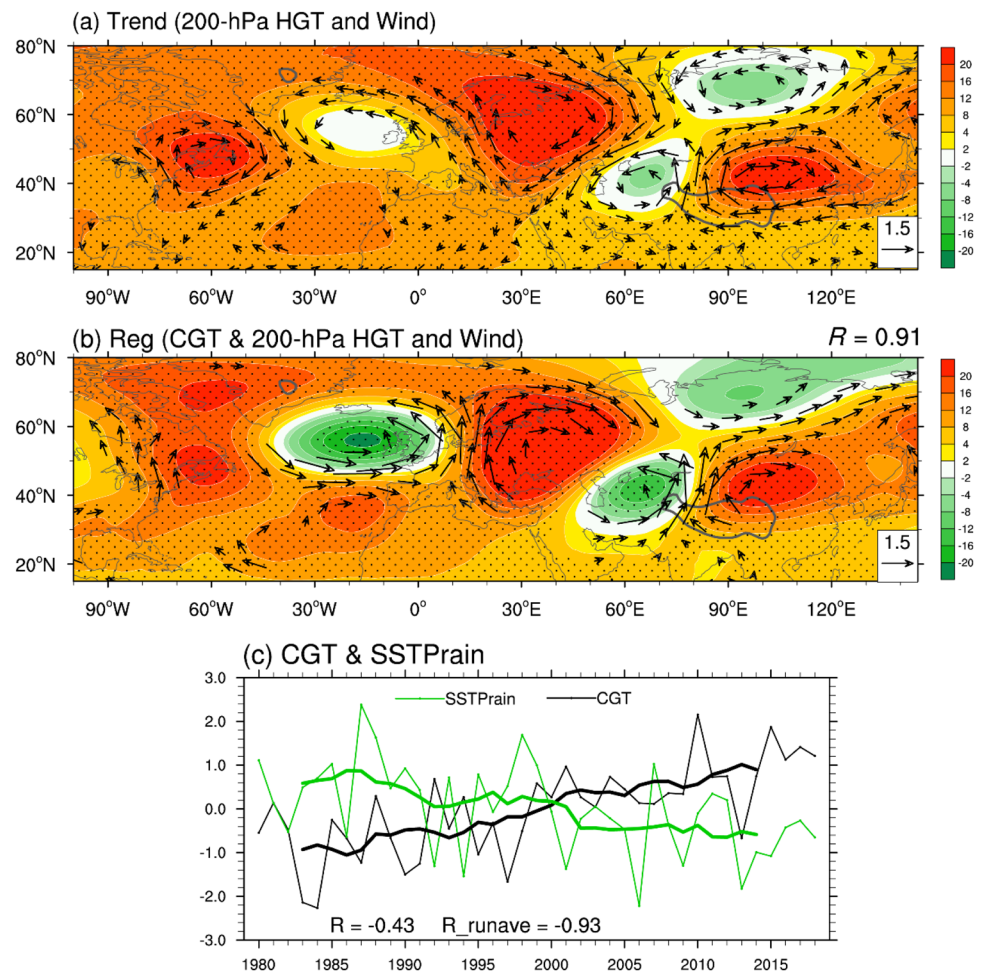
Fig. 6 a Climatology of 350-hPa air temperature (purple contours; K) and specific humidity (shading; g kg^{-1}), and the linear trend of horizontal wind (vectors; $\text{m s}^{-1} \text{decade}^{-1}$) in JAS for 1980–2018. b Linear trend ($\text{W m}^{-2} \text{decade}^{-1}$) for the term $-\langle \mathbf{V}' \cdot \nabla_h(C_p \bar{T}) \rangle$. c Same as b, but for the term $-\langle \mathbf{V}' \cdot \nabla_h(L_v \bar{q}) \rangle$. The stippling indicates the significant values $> 95\%$ confidence level in b and c

term $-\langle \overline{\omega \partial_p h'} \rangle$ is beyond the scope of this paper. We will show the further investigation in a separate study.

3.3 Linkage with the mid-latitude atmospheric change

From both the perspectives of atmospheric circulation analysis and energy balance diagnosis, the foregoing chapter has proved that the trend of descending motion over the SSTP

Fig. 7 **a** Linear trends of 200-hPa geopotential height (shading, m decade^{-1}) and wind (vectors; $\text{m s}^{-1} \text{ decade}^{-1}$) in JAS for 1980–2018. **b** Patterns of regression of 200-hPa geopotential height (shading, m) and wind (vectors, m s^{-1}) against the CGT index. In **a**, **b**, the stippling indicates the significant values > 95% confidence level for geopotential height, and only the significant vectors > 95% confidence level are plotted. Bold gray curves denote the topographic height of 3000 m, and “ $R = 0.91$ ” denotes the spatial correlation coefficient of geopotential height between **a** and **b**. **c** The normalized CGT index (black curve) and GPCP rainfall index over the SSTP area (green curve), and their corresponding 8-year running means (thick lines); “ $R = -0.43$ ” and “ $R_{\text{runave}} = -0.93$ ” denote correlation coefficients for the original and running-mean time series, respectively



can be largely attributed to the upper-level anomalous anticyclone. A further question is, what causes the anticyclonic trend over the northeastern TP during 1980–2018? Fig. 7a shows the linear trend of large-scale atmospheric circulation at 200 hPa in JAS for the recent decades. The anticyclonic trend over the northeastern TP is found not a local phenomenon, but is rather associated with an eastward extension of the large-scale wave train over the North America–North Atlantic–Eurasia region. Meanwhile, the long-term change of upper-level atmospheric circulation in boreal JAS in the CESM-LE is also examined. There exists a similar upstream wave train over the Eurasia in the CESM-LE drying cases (figure not shown). This wave train is analogous to the circumglobal teleconnection (CGT) pattern (its Eurasian portion also called the Silk Road pattern), a stationary mode of boreal summer atmospheric variability in the Eurasian middle latitudes (Ding and Wang 2005; Saeed et al. 2014). With the JRA-55 reanalysis data, the CGT index is calculated as the first principal component (PC1) of the leading mode of 200-hPa meridional wind over the region ($100^{\circ} \text{W}–100^{\circ} \text{E}$, $20^{\circ} \text{N}–80^{\circ} \text{N}$) (Saeed et al., 2014). Figure 7b gives the patterns of regression of 200-hPa geopotential height and wind

against the CGT index, which are extremely similar with the patterns in Fig. 7a. The coefficient of spatial correlation between the geopotential heights in Fig. 7a, b can reach 0.91. Thus, the CGT-like change in atmospheric circulation at middle latitudes in recent decades brought the anticyclonic trend over the northeastern TP. The anomalous anticyclone weakens the upward motion over the SSTP through reducing the upper-level divergence pumping and advecting cold and dry (low moist enthalpy) air into the slope region, finally resulting in the dynamic change in moisture vertical advection and decreased precipitation.

The above corollary is further confirmed by the significant correlation ($R = -0.43$; $P > 99\%$) between the CGT index and the SSTP rainfall index (Fig. 7c). This relationship can also be manifested from the spatial regression of precipitation against the CGT index (Fig. 8). Corresponding with the CGT pattern in mid-latitude atmospheric circulation, all the three precipitation datasets consistently show a significant drying trend in the region of SSTP. Additionally, from the perspective of long-term change, the CGT index shows an upward trend in recent decades, which is exactly contrary to the drying tendency over the SSTP (Fig. 7c).

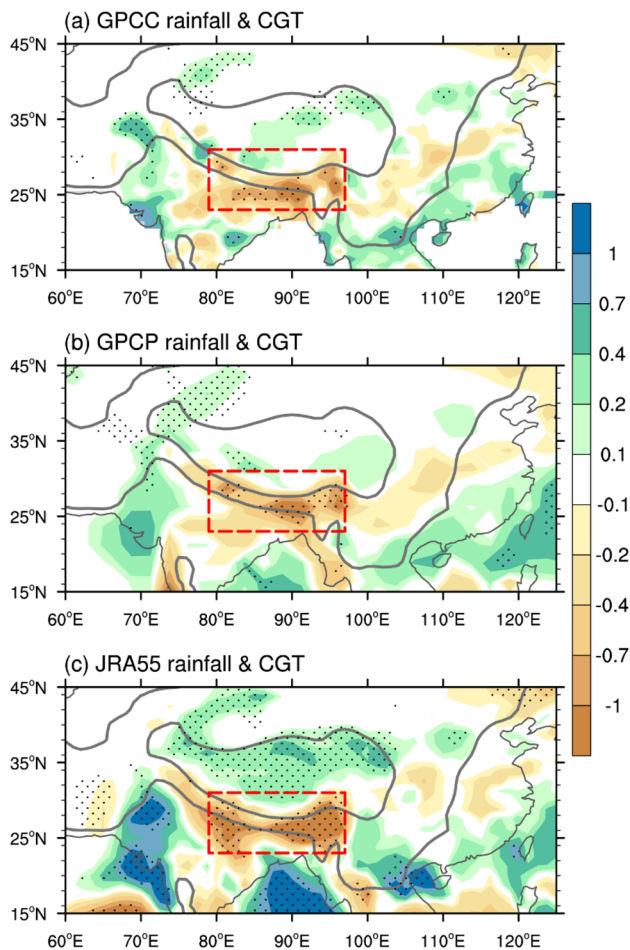


Fig. 8 Patterns of regression of JAS precipitation (mm day^{-1}) against the CGT index in 1980–2018 based on **a** GPCP, **b** GPCP, and **c** JRA55 datasets. The stippling indicates the significant values $>95\%$ the confidence level and the bold gray contours denote the topographic heights of 500 m and 3000 m

4 Discussion and summary

4.1 Discussion

The underlying cause for the mid-latitude atmospheric change with a CGT-like pattern in recent decades is of substantial interest. Limited studies have indicated that the Atlantic Multidecadal Oscillation (AMO) may play a potential role in modulating the decadal variation of the CGT (Lin et al. 2016; Wu et al. 2016a; Hong et al. 2017). However, Wang et al. (2017a) recently reported that the AMO did not show a significant linear relationship with the interdecadal CGT during 1920–2010. In this study, we have reinvestigated the connection between the CGT and the AMO and found that the AMO exhibits a significant correlation ($R=0.45$; $P>99\%$) with the CGT in 1980–2018 (see the supplementary Fig. S4a). Furthermore, the decadal variation of CGT is in phase with that of the AMO (thick

curves in Fig. S4), suggesting that the CGT and AMO are possibly related to each other. In Fig. S4b, it is detected that the CGT trend also connected closely with the sea surface temperature variation in tropical Indian Ocean in the recent decades. However, the associated physical mechanisms for those potential oceanic forcings remain unclear. Besides the oceanic factors, the barotropic instability of the summer mean flow at the exit region of North Atlantic westerly jet is regarded as a source for the maintenance and variation of the CGT (Ding and Wang 2005). We estimate the local barotropic energy conversion CK associated with the CGT following the formula in Simmons et al. (1983). As shown by the supplementary Fig. S5a, significant positive CK in the upper troposphere is clearly observed near the southeastern flank of the Atlantic jet (the exit region), indicating that the CGT wave train can get kinetic energy from the mean flow in this region. More importantly, the CK in that region shows an obvious positive linear trend during the period of 1980–2018 (Fig. S5b). It is thus believed that the barotropic instability in the jet exit region over the North Atlantic also plays a potential role on the long-term change of the CGT. Automatically, further investigation on comprehensively explaining the observed trend of the CGT is still required, since this trend may have led to high-impact extremes in recent boreal summers (Teng and Branstator 2019). Such a study is currently under way and will be reported separately.

Additionally, it was reported that the wave train in CGT pattern may interact with the rainfall anomalies associated the Indian summer monsoon (ISM) at the interannual timescale (e.g., Ding and Wang 2005). One might suspect that the drying trend over the SSTP may be a reason for the mid-latitude CGT-like atmospheric change, rather than a result. We have verified this point using sensitivity experiments with the Community Atmosphere Model, in which the reduced latent heating by 20% (according to the quantified drying) was prescribed over the SSTP. Forced by the weakened heating, an obviously anomalous cyclone appears at the SSTP's upper troposphere (figure not shown). This response of the upper-level atmospheric circulation is similar with the previous simulated results forced by anomalous heating over the southeastern TP with a regional model (see Fig. 7a in Wang et al. 2019) and a nonlinear baroclinic model (see Fig. 4b in Jiang and Ting 2017). From the above, the atmospheric response due to the feedback of the SSTP's drying is very different from the observed dipole pattern with an anticyclonic anomaly over the northeastern TP and a cyclonic anomaly to the west of the TP shown in Fig. 7a, b. Thus, to a large extent, the CGT-like atmospheric change shaped the drying tendency over the SSTP in recent decades more probably, not vice versa. Furthermore, potential feedbacks of the wetting tendency in Northwest India and Bay of Bengal (see Fig. 1d, e) to the formation of the observed CGT-like trend are also numerically examined. Consistent

with a typical Gill-type response (Gill 1980), an upper-tropospheric anticyclonic anomaly forced by the heat source in both two regions (corresponding with the increased precipitation) can be found over the west of the TP (figure not shown). Whereas this anticyclonic response is opposite with the observed cyclonic trend (Fig. 7a). Although the heat source in Northwest India can trigger an anticyclonic anomaly over Northeast Asia, also mentioned by Ding and Wang (2005), its intensity and location are vastly different from the observed anticyclonic trend over the northeastern TP emphasized in this study. In sum, we can infer that the local feedback of the rainfall to the mid-latitude CGT-like atmospheric change is limited.

In the Sect. 3.2, we mentioned that the observed SSTP drying tendency is probably regulated by atmospheric internal variability, instead of anthropogenic forcing. That's because the 40-member ensemble result in the CESM-LE project could not reproduce the decreased precipitation over the SSTP during 1980–2018 (Fig. 4a). Actually, we also have examined the precipitation change in the phase 6 of the Coupled Model Intercomparison Project (CMIP6) with the method of multi-model ensemble (MME). The linear trend of the CMIP6 MME precipitation in JAS for the period of 1980–2018 also presents no drying tendency, but even weak wetting trend appears in the southern and western slope area (Fig. S6a in Supplementary Information). However, under the anthropogenic greenhouse gas forcing, the CMIP6 models consistently project a significant wetting trend over the TP and its slope area in future (Fig. S6b, S6c), which was also produced by the CMIP5 models (e.g., He et al. 2019). Therefore, it can be inferred that the drying SSTP in recent decades was dominated by atmospheric internal variability, such as the mid-latitude CGT-like atmospheric change emphasized in this study. As previous studies have reported, the long-term variations of the CGT pattern across Eurasia in boreal summer was little relevance to the externally forced climate change (e.g., Wang et al. 2017a).

4.2 Summary

Finally, the conclusions obtained from this study are given as follows. A robust drying tendency in the mid-late summer during 1980–2018 is confirmed over the SSTP region using both observational and reanalysis data. According to the ensemble estimation from three precipitation datasets, a nearly 20% decline of the climatological precipitation amount occurred in recent decades, which might exert a negative impact on the water resource for the surrounding countries with densest population of the world. A moisture budget analysis demonstrates that the drying trend over the SSTP is mainly induced by the weakened dynamic component of vertical moisture advection, namely the weakened upward motion over the SSTP. This change in

vertical motion results from the appearance of an upper-level anomalous anticyclone over the northeastern TP, through reducing the divergence field and the pumping effect in the upper troposphere, and also advecting cold and dry air (low moist enthalpy) into the SSTP region. Moreover, it is found that the anticyclonic trend over the northeastern TP is not a local phenomenon, but is rather a portion of the large-scale atmospheric change in middle latitudes that exhibits a CGT-like pattern over the North America–North Atlantic–Eurasia region. In summary, this study highlights the dominate contribution from a CGT-like trend of the mid-latitude atmospheric variability to the drying tendency over the SSTP in recent decades.

Supplementary Information The online version contains supplementary material available at <https://doi.org/10.1007/s00382-022-06262-9>.

Acknowledgements Authors wish to thank Prof. Yi Deng of the Georgia Institute of Technology and Prof. Kun Yang of Tsinghua University for useful discussions, and thank the two anonymous reviewers for their constructive comments. This work was supported jointly by the Guangdong Major Project of Basic and Applied Basic Research (Grant 2020B0301030004), National Natural Science Foundation of China (Grants 41975080, 42088101, and 91637208), Guangdong Province Key Laboratory for Climate Change and Natural Disaster Studies (Grant 2020B1212060025), and the “111-Plan” Project of China (Grant B17049).

Availability of data and material All data and materials used in this manuscript are freely available and comply with field standards.

Declarations

Conflict of interest The authors declare no conflict of interests or competing financial interests.

Open Access This article is licensed under a Creative Commons Attribution 4.0 International License, which permits use, sharing, adaptation, distribution and reproduction in any medium or format, as long as you give appropriate credit to the original author(s) and the source, provide a link to the Creative Commons licence, and indicate if changes were made. The images or other third party material in this article are included in the article's Creative Commons licence, unless indicated otherwise in a credit line to the material. If material is not included in the article's Creative Commons licence and your intended use is not permitted by statutory regulation or exceeds the permitted use, you will need to obtain permission directly from the copyright holder. To view a copy of this licence, visit <http://creativecommons.org/licenses/by/4.0/>.

References

- Adler RF, Huffman GJ, Chang A, Ferrara R, Xie P-P, Janowiak J et al (2003) The version-2 global precipitation climatology project (GPCP) monthly precipitation analysis (1979–present). *J Hydro-meteorol* 4:1147–1167
- Back L, Bretherton C (2006) Geographic variability in the export of moist static energy and vertical motion profiles in the tropical Pacific. *Geophys Res Lett* 33:L17810

- Boos W, Kuang Z (2010) Dominant control of the South Asian monsoon by orographic insulation versus plateau heating. *Nature* 463:218–223
- Chou C, Neelin J (2004) Mechanisms of global warming impacts on regional tropical precipitation. *J Clim* 17(13):2688–2701
- Ding Q, Wang B (2005) Circumglobal teleconnection in the northern Hemisphere summer. *J Clim* 18:3483–3505
- Ding Q, Schweiger A, L'Heureux M, Battisti D, Po-Chedley S, Johnson N (2017) Influence of high-latitude atmospheric circulation changes on summertime Arctic sea ice. *Nat Clim Change* 7:289–296
- Duan A, Li F, Wang M, Wu G (2011) Persistent weakening trend in the spring sensible heat source over the Tibetan Plateau and its impact on the Asian summer monsoon. *J Clim* 24:5671–5682
- Duan A, Wu G, Liu Y, Ma Y, Zhao P (2012) Weather and climate effects of the Tibetan Plateau. *Adv Atmos Sci* 29:978–992
- Gao Y, Cuo L, Zhang Y (2014) Changes in moisture flux over the Tibetan Plateau during 1979–2011 and possible mechanisms. *J Clim* 27:1876–1893
- Gao Y, Li X, Leung R, Chen D, Xu J (2015) Aridity changes in the Tibetan Plateau in a warming climate. *Environ Res Lett* 10:034013
- Gill AE (1980) Some simple solutions for heat-induced tropical circulation. *Q J R Meteorol Soc* 106:447–462
- He C, Wang Z, Zhou T, Li T (2019) Enhanced latent heating over the Tibetan Plateau as a key to the enhanced East Asian summer monsoon circulation under a warming climate. *J Clim* 32:3373–3388
- Hill S (2019) Theories for past and future monsoon rainfall changes. *Curr Clim Change Rep* 5:160–171
- Hong X, Lu R, Li S (2017) Amplified summer warming in Europe–West Asia and Northeast Asia after the mid-1990s. *Environ Res Lett* 12:094007
- Hsu H, Liu X (2003) Relationship between the Tibetan Plateau heating and East Asian summer monsoon rainfall. *Geophys Res Lett* 30:2066
- Hu S, Zhou T, Wu B (2021) Impact of developing ENSO on Tibetan Plateau summer rainfall. *J Clim* 34:3385–3400
- Huffman G, Bolvin D, Nelkin E, Wolff D, Adler R, Gu G et al (2007) The TRMM multisatellite precipitation analysis (TMPA): quasi-global, multiyear, combined-sensor precipitation estimates at fine scale. *J Hydrometeorol* 8:38–55
- Hui C, Zheng X (2018) Uncertainty in Indian Ocean Dipole response to global warming: the role of internal variability. *Clim Dyn* 51:3597–3611
- Jiang X, Ting M (2017) A dipole pattern of summertime rainfall across the Indian subcontinent and the Tibetan Plateau. *J Clim* 30:9607–9620
- Kay JE, Deser C, Phillips A, Mai A, Hannay C, Strand G et al (2015) The Community Earth System Model (CESM) large ensemble project: a community resource for studying climate change in the presence of internal climate variability. *Bull Am Meteorol Soc* 96:1333–1349
- Kitoh A (2004) Effects of mountain uplift on East Asian summer climate investigated by a coupled atmosphere–ocean GCM experiments. *J Clim* 17:783–802
- Kobayashi S, Ota Y, Harada Y, Ebata A, Moriya M, Onoda H et al (2015) The JRA-55 Reanalysis: General specifications and basic characteristics. *J Meteorol Soc Jpn* 93:5–48
- Li L, Yang S, Wang Z, Zhu X, Tang H (2010) Evidence of warming and wetting climate over the Qinghai-Tibet Plateau. *Arct Antarct Alp Res* 42:449–457
- Li Z, Lau KM, Ramanathan V, Wu G, Ding Y, Manoj MG et al (2016) Aerosol and monsoon climate interactions over Asia. *Rev Geophys* 54:866–929
- Lin S, Wu B, Zhou T (2016) Is the interdecadal circumglobal teleconnection pattern excited by the Atlantic Multidecadal Oscillation? *Atmos Ocean Sci Lett* 9:451–457
- Liu X, Yin Z (2001) Spatial and temporal variation of summer precipitation over the eastern Tibetan Plateau and the North Atlantic Oscillation. *J Clim* 14:2896–2909
- Liu B, Wu G, Mao J, He J (2013) Genesis of the South Asian high and its impact on the Asian summer monsoon onset. *J Clim* 26:2976–2991
- Liu H, Duan K, Li M, Shi P, Yang J, Zhang X, Sun J (2015) Impact of the North Atlantic Oscillation on the dipole oscillation of summer precipitation over the central and eastern Tibetan Plateau. *Int J Climatol* 35:4539–4546
- Liu Y, Chen H, Hu X (2021) The unstable relationship between the precipitation dipole pattern in the Tibetan Plateau and summer NAO. *Geophys Res Lett* 48:e2020GL091941
- Lu C, Yu G, Xie G (2005) Tibetan Plateau serves as a water tower. *IEEE Int Geosci Remote Sens Sympos* 5:3120–3123
- Lu M, Yang S, Li Z, He B, He S, Wang Z (2018) Possible effect of the Tibetan Plateau on the “upstream” climate over West Asia, North Africa, South Europe and the North Atlantic. *Clim Dyn* 51:1485–1498
- Lu M, Huang B, Li Z, Yang S, Wang Z (2019) Role of Atlantic air–sea interaction in modulating the effect of Tibetan Plateau heating on the upstream climate over Afro-Eurasia–Atlantic regions. *Clim Dyn* 53:509–519
- Mason R, Anderson C (1963) The development and decay of the 100-mb summertime anticyclone over southern Asia. *Mon Weather Rev* 91:3–12
- Neelin J, Held I (1987) Modeling tropical convergence based on the moist static energy budget. *Mon Weather Rev* 115:3–12
- Neelin J, Chou C, Su H (2003) tropical drought regions in global warming and El Niño teleconnections. *Geophys Res Lett* 30(24):2275
- Peng D, Zhou T (2017) Why was the arid and semiarid northwest China getting wetter in the recent decades? *J Geophys Res Atmos* 122:9060–9075
- Poudel DD, Duex TW (2017) Vanishing springs in Nepalese mountains: assessment of water sources, farmers’ perceptions, and climate change adaptation. *Mt Res Dev* 37:35–46
- Saeed S, Lipzig N, Müller W, Saeed F, Zanchettin D (2014) Influence of the circumglobal wave-train on European summer precipitation. *Clim Dyn* 43:503–515
- Schneider U, Becker A, Finger P, Meyer-Christoffer A, Ziese M, Rudolf B (2014) GPCC’s new land surface precipitation climatology based on quality-controlled in situ data and its role in quantifying the global water cycle. *Theor Appl Climatol* 115:15–40
- Simmons AJ, Wallace JM, Branstator GW (1983) Barotropic wave propagation and instability, and atmospheric teleconnection patterns. *J Atmos Sci* 40:1363–1392
- Sun J, Yang K, Guo W, Wang Y, He J, Lu H (2020) Why has the Inner Tibetan Plateau become wetter since the mid-1990s? *J Clim* 33:8507–8522
- Teng H, Branstator G (2019) Amplification of waveguide teleconnections in the boreal summer. *Curr Clim Change Rep* 5:421–432
- Wang S-Y, Gillies R (2013) Influence of the Pacific quasi-decadal oscillation on the monsoon precipitation in Nepal. *Clim Dyn* 40:95–107
- Wang Z, Duan A, Wu G, Yang S (2016) Mechanism for occurrence of precipitation over the southern slope of the Tibetan Plateau without local surface heating. *Int J Climatol* 36:4164–4171
- Wang L, Xu P, Chen W, Liu Y (2017a) Interdecadal variations of the silk road pattern. *J Clim* 30:9915–9932
- Wang Z, Duan A, Yang S, Ullah K (2017b) Atmospheric moisture budget and its regulation on the variability of summer precipitation over the Tibetan Plateau. *J Geophys Res Atmos* 122:614–630

- Wang Z, Yang S, Duan A, Hua W, Ullah K, Liu S (2019) Tibetan Plateau heating as a driver of monsoon rainfall variability in Pakistan. *Clim Dyn* 52:6121–6130
- Wu G, Liu Y, He B, Bao Q, Duan A, Jin F (2012) Thermal controls on the Asian summer monsoon. *Sci Rep* 2:404
- Wu B, Lin J, Zhou T (2016a) Interdecadal circumglobal teleconnection pattern during boreal summer. *Atmos Sci Lett* 17:446–452
- Wu G, Zhuo H, Wang Z, Liu Y (2016b) Two types of summertime heating over the Asian large-scale orography and excitation of potential-vorticity forcing I. Over the Tibetan Plateau. *Sci China Earth Sci* 59:1996–2008
- Wu Z, Zhang P, Chen H, Li Y (2016c) Can the Tibetan Plateau snow cover influence the interannual variations of Eurasian heat wave frequency? *Clim Dyn* 46:3405–3417
- Wu B, Zhou T, Li T (2017) Atmospheric dynamic and thermodynamic processes driving the western North Pacific anomalous anticyclone during El Niño. Part I: maintenance mechanisms. *J Clim* 30:9621–9635
- Xu X, Lu C, Shi X, Gao S (2008) World water tower: an atmospheric perspective. *Geophys Res Lett* 35:L20815
- Yang K, Wu H, Qin J, Lin C, Tang W, Chen Y (2014) Recent climate changes over the Tibetan Plateau and their impacts on energy and water cycle: a review. *Glob Planet Change* 112:79–91
- Yao T, Thompson L, Yang W, Yu W, Gao Y, Guo X et al (2012) Different glacier status with atmospheric circulations in Tibetan Plateau and surroundings. *Nat Clim Change* 2:663–667
- Yatagai A, Kamiguchi K, Arakawa O, Hamada A, Yasutomi N, Kitoh A (2012) APHRODITE: constructing a long-term daily gridded precipitation dataset for Asia based on a dense network of rain gauges. *Bull Am Meteorol Soc* 93:1401–1415
- Ye D-Z, Wu G (1998) The role of the heat source of the Tibetan Plateau in the general circulation. *Meteorol Atmos Phys* 67:181–198
- You Q, Min J, Zhang W, Pepin N, Kang S (2015) Comparison of multiple datasets with gridded precipitation observations over the Tibetan Plateau. *Clim Dyn* 45:791–806
- Yue S, Wang B, Yang K, Xie Z, Lu H, He J (2020) Mechanisms of the decadal variability of monsoon rainfall in the southern Tibetan Plateau. *Environ Res Lett* 16:014011
- Zangvil A, Portis DH, Lamb PJ (2004) Investigation of the large-scale atmospheric moisture field over the midwestern United States in relation to summer precipitation. Part II: recycling of local evapotranspiration and association with soil moisture and crop yields. *J Clim* 17:3283–3301
- Zhang L, Su F, Yang D et al (2013) Discharge regime and simulation for the upstream of major rivers over Tibetan Plateau. *J Geophys Res Atmos* 118:8500–8518
- Zhang C, Tang Q, Chen D (2017a) Recent changes in the moisture source of precipitation over the Tibetan Plateau. *J Clim* 30:1807–1819
- Zhang G, Yao T, Shum CK, Yi S, Yang K, Xie H et al (2017b) Lake volume and groundwater storage variations in Tibetan Plateau's endorheic basin. *Geophys Res Lett* 44:5550–5560
- Zhang G, Luo W, Chen W, Zheng G (2019) A robust but variable lake expansion on the Tibetan Plateau. *Sci Bull* 64:1306–1309
- Zhao P, Chen L (2001) Climatic features of atmospheric heat source/sink over the Qinghai-Xizang Plateau in 35 years and its relation to rainfall in China. *Sci China Ser D* 44:858–864

Publisher's Note Springer Nature remains neutral with regard to jurisdictional claims in published maps and institutional affiliations.